INTERNATIONAL JOURNAL FOR NUMERICAL METHODS IN ENGINEERING
Int. J. Numer. Meth. Engng 2005; **63**:197–217
Published online 15 February 2005 in Wiley InterScience (www.interscience.wiley.com). DOI: 10.1002/nme.1276

Insight into the flow-condition-based interpolation finite element approach: solution of steady-state advection–diffusion problems

Haruhiko Kohno and Klaus Jürgen Bathe*, †

Department of Mechanical Engineering, Massachusetts Institute of Technology, 77 Massachusetts Avenue, Cambridge, MA, 02139-4307, U.S.A.

SUMMARY

The flow-condition-based interpolation (FCBI) finite element approach is studied in the solution of advection–diffusion problems. Two FCBI procedures are developed and tested with the original FCBI method: in the first scheme, a general solution of the advection–diffusion equation is embedded into the interpolation, and in the second scheme, the link-cutting bubbles approach is used in the interpolation. In both procedures, as in the original FCBI method, no artificial parameters are included to reach stability for high Péclet number flows. The procedures have been implemented for two-dimensional analysis and the results of some test problems are presented. These results indicate good stability and accuracy characteristics and the potential of the FCBI solution approach. Copyright © 2005 John Wiley & Sons, Ltd.

KEY WORDS: advection–diffusion; stabilization; flow-condition-based interpolations

1. INTRODUCTION

The numerical solution of high Péclet and high Reynolds number flows is of great importance in research and industry. For this reason and because the development presents a great challenge, a very large research effort has been focused on improving the methods of solution over the last decades, and this effort is still continuing very widely.

The finite element method is clearly the most effective numerical solution technique for the analysis of solids and structures [1, 2]. However, considering fluid flows, while much research has been focused on the development of finite element methods (see, e.g. References [1–7]), finite difference, finite volume and spectral methods are still considerably more effective in most practical applications. Indeed, almost all fluid flow problems in industry are still solved

*Correspondence to: K. J. Bathe, Department of Mechanical Engineering, Massachusetts Institute of Technology, 77 Massachusetts Avenue, Cambridge, MA, 02139-4307, U.S.A.
†E-mail: kjb@mit.edu

Contract/grant sponsor: Ministry of Education, Culture, Sports, Science and Technology (MEXT), Japan

Received 5 May 2004
Revised 9 July 2004
Accepted 8 November 2004

using finite volume techniques. On the other hand, if a finite element method were available that is clearly more effective, then such a method would find wide usage.

We have focused our research on the development of the flow-condition-based interpolation (FCBI) procedure [8–10] for the finite element solution of incompressible fluid flows, including fluid–structure interactions. This method might be referred to as a hybrid of the traditional finite element and finite volume methods. The key aspects of the FCBI procedure are that, firstly, finite element interpolations considering flow conditions are used which lead to stability and, secondly, local flux equilibrium (that is, mass and momentum conservation) is satisfied. Our objective in this development is to reach a method that is more effective in stability, accuracy and computational effort than the traditional finite element and finite volume techniques.

Specifically, the basic aim in our development is to reach a numerical scheme that is stable with optimal accuracy characteristics, for low and high Péclet and Reynolds number flows [8–11]. In particular, considering a high Reynolds number flow, the scheme should give a reasonable solution, even when using a rather coarse mesh and without the use of artificial solution parameters. The global flow characteristics should be correctly displayed, and in fluid–structure interactions, the tractions on the structural surfaces should be reasonable. As the fluid mesh is then refined, more details of the flow should be revealed, and ideally the numerical solution would converge with optimum rate to the 'exact' solution of the mathematical model. In practice, of course, the solution of the Navier–Stokes equations at high Reynolds number would not be obtained with high accuracy. The mesh would have to be too fine. Instead, a turbulence model would be used at some stage of mesh refinement. However, the solution property that stability is preserved at high Reynolds and Péclet number flows with coarse meshes and optimal accuracy is of much value in practical analysis.

The possible use of coarse meshes without artificial solution parameters implies that an analyst does not need to spend undue effort on meshing the domain and experimenting with numerical parameters merely to obtain a first reasonable flow solution. Also, if a discretization scheme is employed with goal-oriented error measures [12], then it is assumed that solutions can directly be obtained for all meshes used. The goal-oriented discretization approach is particularly valuable in the solution of fluid–structure interactions where the fluid mesh only needs to be fine enough to solve accurately for the pressure/tractions on the structure.

The basic philosophy of our developments was presented earlier [8–10], and the FCBI approach is already quite widely used [10]. However, we are of course aiming to further study the solution properties and increase the effectiveness of the original procedure. Since the method is a hybrid of the finite element and finite volume techniques, the FCBI scheme is naturally also related to the much researched streamline upwind/Petrov–Galerkin (SUPG) method [3], the Galerkin/least-squares (GLS) method [4], the use of bubble functions [6], and other schemes [1, 2, 7]. However, a distinguishing feature is that an analytical solution of the one-dimensional advection–diffusion equation (to stabilize the convective terms in the Galerkin formulation) is used over a control volume, and hence the FCBI method is also related to the cubic interpolated pseudoparticle/propagation (CIP) method [13].

The objective of this paper is to study the spatial solution accuracy of the original FCBI scheme [9] and two variations thereof for advection–diffusion problems in order to obtain further insight into the solution approach. Whereas in the original FCBI scheme one-dimensional analytical flow conditions are used in two- and three-dimensional interpolations, we consider here, in an additional FCBI scheme, a general two-dimensional solution. Furthermore, in a third scheme we embed the interpolations of the link-cutting bubbles proposed by Brezzi *et al*. [14]

into the FCBI approach. In the paper, we first present the numerical procedures used and then give the solutions of various test problems. The numerical experiments indicate the stability and accuracy of the FCBI procedures and also show that the FCBI approach has significant further potential to reach improved solution methods.

2. FCBI METHODS FOR ADVECTION–DIFFUSION PROBLEMS

In this section we review the original FCBI method and introduce two additional FCBI procedures. We consider an incompressible flow advection–diffusion problem in a two-dimensional domain in which the velocity is prescribed. A steady-state analysis is carried out with Dirichlet boundary conditions. We assume that the problem is well-posed in the Hilbert space Θ. The non-dimensional governing equation in conservative form is:

Find the temperature $\theta(\mathbf{x}) \in \Theta$ such that

$$\nabla \cdot \left(\mathbf{v}\theta - \frac{1}{Pe} \nabla\theta \right) = 0, \quad \mathbf{x} \in \Omega \tag{1}$$

where $\mathbf{v}$ is the prescribed velocity and $\Omega \in \Re^2$ is a domain with boundary $S = \bar{S}_\theta$. The Péclet number is defined as $Pe = UL/\alpha$; U, L and α are the representative velocity, the representative length and the thermal diffusivity, respectively. The above equation is subject to the following boundary condition:

$$\theta = \theta^s, \quad \mathbf{x} \in \bar{S}_\theta \tag{2}$$

where θ^s is the prescribed temperature on the boundary $\bar{S}_\theta$.

2.1. The original method

For the finite element solution, we use a Petrov–Galerkin variational formulation with subspaces Φ_h, Θ_h and W_h of Θ of the problem in Equations (1) and (2). The formulation for the numerical solution is

Find $\phi \in \Phi_h$, $\theta \in \Theta_h$ such that for all $w \in W_h$

$$\int_\Omega w \left\{ \nabla \cdot \left(\mathbf{v}\phi - \frac{1}{Pe} \nabla\theta \right) \right\} \mathrm{d}\Omega = 0 \tag{3}$$

Figure 1(a) shows a mesh of elements in the natural co-ordinate system. Here, both velocity and temperature are defined at each node of the 4-node elements.

The weight functions in the space W_h are step functions. For example, we have at node 1 in Figure 1(b),

$$h_1^w = \begin{cases} 1 & (\xi, \eta) \in \left[0,\ \frac{1}{2}\right] \times \left[0,\ \frac{1}{2}\right] \\ 0 & \text{else} \end{cases} \tag{4}$$

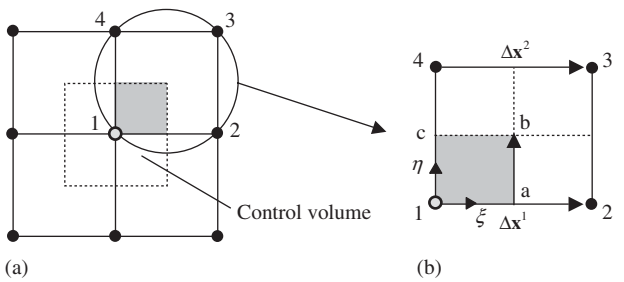

Figure 1. Control volume on the 4-node elements and evaluation of functions in Φ_h for flux through ab: (a) 4-node elements; and (b) flux through ab.

This corresponds to the finite volume discretization, in which the flux is evaluated on the sides of the control volumes. The use of the control volumes enforces the local conservation of flux and helps to provide stability and accuracy in the numerical solution.

The trial functions in Θ_h are the bilinear interpolation functions defined as

$$\begin{bmatrix} h_1^\theta & h_4^\theta \\ h_2^\theta & h_3^\theta \end{bmatrix} = \mathbf{h}(\xi)\mathbf{h}^{\mathrm{T}}(\eta) \tag{5}$$

where $\mathbf{h}^{\mathrm{T}}(y) = [1-y,\ y]$ ($y = \xi, \eta$ with $0 \leqslant \xi, \eta \leqslant 1$). In order to reach a stable solution, the trial functions in Φ_h are defined considering the flow conditions along each side of the elements. The functions are for the flux through ab in Figure 1(b),

$$\begin{bmatrix} h_1^\phi & h_4^\phi \\ h_2^\phi & h_3^\phi \end{bmatrix} = \left[\mathbf{h}\left(x^1\right), \mathbf{h}\left(x^2\right)\right] \mathbf{h}(\eta)\mathbf{h}^{\mathrm{T}}(\eta) \tag{6}$$

with

$$\begin{aligned} x^k &= \frac{\mathrm{e}^{q^k \xi} - 1}{\mathrm{e}^{q^k} - 1}, \quad q^k = Pe(\bar{\mathbf{v}}^k \cdot \Delta\mathbf{x}^k) \\ \bar{\mathbf{v}}^1 &= \tfrac{1}{2}(\mathbf{v}_1 + \mathbf{v}_2), \quad \bar{\mathbf{v}}^2 = \tfrac{1}{2}(\mathbf{v}_3 + \mathbf{v}_4) \\ \Delta\mathbf{x}^1 &= \mathbf{x}_2 - \mathbf{x}_1, \quad \Delta\mathbf{x}^2 = \mathbf{x}_3 - \mathbf{x}_4 \end{aligned} \tag{7}$$

where $\bar{\mathbf{v}}^k$ is the average velocity evaluated at the centre of the sides considered ($\xi = 1/2$ and $\eta = 0, 1$ for $k = 1, 2$, respectively) and is calculated using the nodal velocity variables $\mathbf{v}_i$; $\mathbf{x}_i$ are the position vectors at the nodes. Similarly, the functions for the flux through bc are obtained by using the flow conditions on the corresponding sides. When the Péclet number is small enough, the variable x^k approaches the natural co-ordinate value ξ. This is easily confirmed by substituting the following approximation into Equation (7), $\mathrm{e}^{q^k} \cong 1 + q^k$.

Using Equations (5)–(7) the temperatures ϕ and θ are, respectively, calculated with the trial functions in Φ_h and Θ_h as follows:

$$\phi = h_i^{\phi}\theta_i \tag{8}$$

$$\theta = h_i^{\theta}\theta_i \tag{9}$$

where θ_i are the nodal temperature variables. The trial functions used here satisfy the requirement $\Sigma h_i = 1$. The flux is calculated with the interpolated values at the centre of the sides of the control volumes. For example, the flux through ab is obtained as follows:

$$\int_a^b \mathbf{n}\cdot\mathbf{f}\,\mathrm{d}s = (\mathbf{n}\cdot\mathbf{f})|_{\xi=1/2,\eta=1/4}\Delta s_{\mathrm{ab}} \tag{10}$$

with

$$\mathbf{f}(\xi,\eta) = \mathbf{v}\phi - \frac{1}{Pe}\,\mathbf{g}^j\,\frac{\partial\theta}{\partial\xi^j} \tag{11}$$

where $\mathbf{n}$, Δs_{ab} and $\mathbf{g}^j$ are the unit normal vector pointing to the outside of the control volume, the length of ab and the contravariant base vector, respectively. In Equation (10), the velocity is interpolated with the trial functions in Θ_h; $\mathbf{v} = h_i^{\theta}\mathbf{v}_i$.

This approach of solution was first introduced into the Navier–Stokes equations with the primary aim to have stability of the solution [9, 15], because in practice a stable and reasonable solution is ideally obtained at any Reynolds (and Péclet) number flow. Of course, we also endeavour to have a solution as accurate as possible, and this aim motivates the further development of the scheme.

2.2. Using a general solution

In the advection-dominated regime, an effective stabilizing scheme is required in order to obtain reliable results with a reasonable mesh. This requirement is fulfilled in the original FCBI method in a physically based manner by introducing the one-dimensional exact solution of the advection–diffusion equation into the trial functions in Φ_h as shown in Equations (6) and (7). However, since the flow conditions are estimated on the sides of the elements and then linearly interpolated in the elements, fine grids are necessary to obtain accurate results when very high Péclet number flows are analysed in multi-dimensional domains. For this reason, possibly more efficient trial functions in Φ_h, which are based on two-dimensional flow conditions, are considered in this section.

In two-dimensional analysis, it is not possible to obtain the exact solution of the advection–diffusion equation in an element since the exact boundary conditions on the sides are unknown as long as the temperatures are defined only at the nodes. Hence, the following trial functions are created by multiplying the one-dimensional exact-solution-based interpolation in the ξ direction by that in the η direction, which are in an analogous form with Equation (5):

$$\begin{bmatrix} h_1^{\phi} & h_4^{\phi} \\ h_2^{\phi} & h_3^{\phi} \end{bmatrix} = \mathbf{h}(\alpha)\mathbf{h}^{\mathrm{T}}(\beta) \tag{12}$$

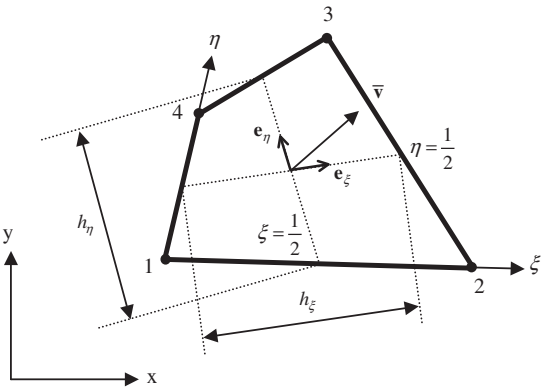

Figure 2. Illustration of the projections of velocity and the element lengths in the ξ and η directions.

with

$$\alpha=\frac{\mathrm{e}^{Pe^e_\xi\xi}-1}{\mathrm{e}^{Pe^e_\xi}-1},\quad \beta=\frac{\mathrm{e}^{Pe^e_\eta\eta}-1}{\mathrm{e}^{Pe^e_\eta}-1}$$

$$Pe^e_\xi=Pe\left(\bar{\mathbf{v}}\cdot\mathbf{e}_\xi\right)h_\xi=Pe\,\bar{v}_\xi h_\xi,\quad Pe^e_\eta=Pe\left(\bar{\mathbf{v}}\cdot\mathbf{e}_\eta\right)h_\eta=Pe\,\bar{v}_\eta h_\eta$$

$$h_\xi=\frac{\left\|\Delta\mathbf{x}^1+\Delta\mathbf{x}^2\right\|}{2},\quad h_\eta=\frac{\left\|\Delta\mathbf{y}^1+\Delta\mathbf{y}^2\right\|}{2} \tag{13}$$

$$\Delta\mathbf{y}^1=\mathbf{x}_4-\mathbf{x}_1,\quad \Delta\mathbf{y}^2=\mathbf{x}_3-\mathbf{x}_2$$

where Pe^e_ξ and Pe^e_η are the element Péclet numbers corresponding to the projections of the velocity vector $\bar{\mathbf{v}}$ evaluated at the centre of the element onto the ξ and η directions, see Figure 2.

It should be emphasized that in a rectangular element the above trial functions correspond to the two-dimensional general solution which consists of four independent basic solutions connected linearly as follows:

$$\phi=\left[1,\mathrm{e}^{Pe^e_\xi\xi},\mathrm{e}^{Pe^e_\eta\eta},\mathrm{e}^{Pe^e_\xi\xi+Pe^e_\eta\eta}\right]\begin{bmatrix}C_1\\C_2\\C_3\\C_4\end{bmatrix} \tag{14}$$

Equations (8), (12) and (13) are obtained by substituting the following boundary conditions into Equation (14): $\theta_1=\theta(0,0)$, $\theta_2=\theta(1,0)$, $\theta_3=\theta(1,1)$, $\theta_4=\theta(0,1)$. Note that these trial functions also meet the requirement $\Sigma h_i=1$ regardless of the element Péclet numbers.

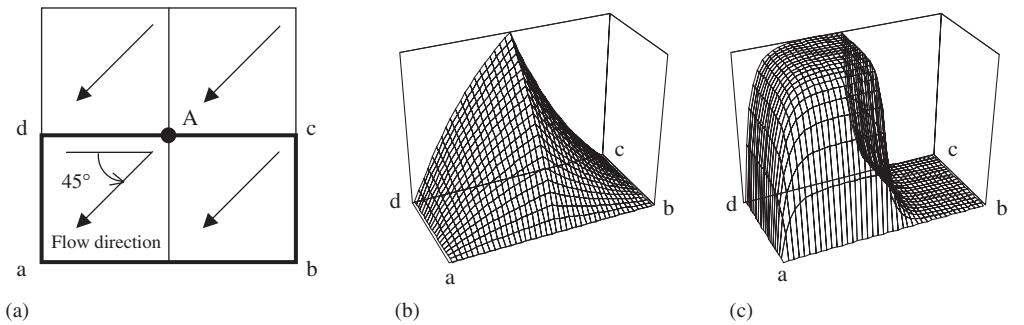

Figure 3. Trial functions in Φ_h for node A in two elements: (a) problem definition; (b) $Pe^e = 1$; and (c) $Pe^e = 10$.

Figure 3 shows the profiles of the trial functions for $Pe^e = Pe^e_\xi = Pe^e_\eta = 1, 10$ in two elements in case a 45° advective velocity is prescribed. When the element Péclet numbers are small enough, the trial functions in Equation (12) approach the bilinear interpolation functions in Equation (5) since $\mathrm{e}^{Pe^e_\xi} \cong 1 + Pe^e_\xi$, $\mathrm{e}^{Pe^e_\eta} \cong 1 + Pe^e_\eta$. Of course, using the same procedure, the proposed trial functions can, also, be developed directly for three-dimensional solutions.

2.3. Using link-cutting bubbles

Another approach to stabilize the solution can be established by adopting an augmented strategy, in which the finite element space is enriched by bubble functions. In this section, we propose a scheme that introduces the link-cutting bubbles [14], suitably located in the augmented space considering flow conditions, into the FCBI procedure.

Consider a one-dimensional advection–diffusion problem solved with 2-node equal length elements. Here, the element Péclet number is positive and we define it to be $q^k/2$. In this case, the exponential scheme [16], which gives the exact solution at each node, can be written as follows:

$$-\mathrm{e}^{q^k/2}\theta_{j-1} + \left(\mathrm{e}^{q^k/2} + 1\right)\theta_j - \theta_{j+1} = 0 \tag{15}$$

where θ_{j-1}, θ_j and θ_{j+1} are the temperature variables at the consecutive nodes. Then the variable θ_j is obtained in terms of θ_{j-1} and θ_{j+1} as follows:

$$\theta_j = \frac{\mathrm{e}^{q^k} - \mathrm{e}^{q^k/2}}{\mathrm{e}^{q^k} - 1}\,\theta_{j-1} + \frac{\mathrm{e}^{q^k/2} - 1}{\mathrm{e}^{q^k} - 1}\,\theta_{j+1} = \mathbf{h}^{\mathrm{T}}\left(x^k(1/2)\right)\begin{bmatrix}\theta_{j-1}\\ \theta_{j+1}\end{bmatrix} \tag{16}$$

Note that Equation (16) contains the same vector $\mathbf{h}\left(x^k\right)$ that is used in Equation (6), when $\xi = 1/2$. Similarly, the following equation is obtained in the Galerkin method coupled with the link-cutting bubbles:

$$\left(-\frac{q^k}{4} - 1 - \frac{q^k}{2}U\right)\theta_{j-1} + 2\left(1 + \frac{q^k}{2}U\right)\theta_j + \left(\frac{q^k}{4} - 1 - \frac{q^k}{2}U\right)\theta_{j+1} = 0 \tag{17}$$

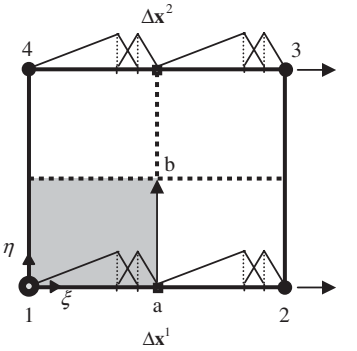

Figure 4. Evaluation of the trial functions based on link-cutting bubbles in Φ_h for flux through ab.

where the term $q^k U/2$ represents the stabilizing effect. Then the variable θ_j is obtained as follows:

$$\theta_j = \frac{q^k + 4 + 2q^k U}{8 + 4q^k U}\,\theta_{j-1} + \frac{-q^k + 4 + 2q^k U}{8 + 4q^k U}\,\theta_{j+1} = \mathbf{h}^{\mathrm{T}}(b^k)\begin{bmatrix}\theta_{j-1}\\ \theta_{j+1}\end{bmatrix} \tag{18}$$

with

$$b^k = \frac{-q^k + 4 + 2q^k U}{8 + 4q^k U} \tag{19}$$

Therefore, this bubble stabilization technique can be naturally introduced into the original FCBI method by replacing x^k in Equation (7) with b^k. When the link-cutting bubbles are set on the vectors $\Delta\mathbf{x}^1$ and $\Delta\mathbf{x}^2$ as shown in Figure 4, at $\xi = 1/2$ the trial functions in Φ_h are for the flux through ab,

$$\begin{bmatrix} h_1^\phi & h_4^\phi \\ h_2^\phi & h_3^\phi \end{bmatrix} = \left[\mathbf{h}\left(b^1\right), \mathbf{h}\left(b^2\right)\right]\mathbf{h}(\eta)\mathbf{h}^{\mathrm{T}}(\eta) \tag{20}$$

$$\text{if } u^k \geqslant 0 \quad \text{then } b^k = \frac{-\left|q^k\right| + 4 + 2\left|q^k\right| U}{8 + 4\left|q^k\right| U} \tag{21}$$

$$\text{if } u^k < 0 \quad \text{then } b^k = \frac{\left|q^k\right| + 4 + 2\left|q^k\right| U}{8 + 4\left|q^k\right| U} \tag{22}$$

with

$$U = \frac{d_1\left(d_1 S_{2,2} - d_2 S_{1,2}\right) - d_2\left(d_1 S_{2,1} - d_2 S_{1,1}\right)}{S_{1,1}S_{2,2} - S_{1,2}S_{2,1}}\,|u^k|$$

$$d_1 = \frac{1}{l^k}\left(\frac{\kappa^k}{2} + \frac{\delta^k}{2}\right), \quad d_2 = \frac{1}{l^k}\left(\frac{\delta^k}{2} + \frac{\lambda^k}{2}\right)$$

$$S_{1,1} = \frac{1}{Pe}\left(\frac{1}{\kappa^k} + \frac{1}{\delta^k}\right), \quad S_{1,2} = -\frac{1}{Pe\delta^k} + \frac{|u^k|}{2}$$

$$S_{2,1} = -\frac{1}{Pe\delta^k} - \frac{|u^k|}{2}, \quad S_{2,2} = \frac{1}{Pe}\left(\frac{1}{\delta^k} + \frac{1}{\lambda^k}\right)$$

$$l^k = \frac{\|\Delta\mathbf{x}^k\|}{2}, \quad u^k = \frac{\bar{\mathbf{v}}^k \cdot \Delta\mathbf{x}^k}{\|\Delta\mathbf{x}^k\|} \tag{23}$$

The two-bubble subgrid is determined by putting two points, $\mathbf{z}_1^k$, $\mathbf{z}_2^k$, in the half length of each side as follows:

$$\text{if } \frac{6}{Pe} \geqslant |u^k| l^k \quad \text{then } \kappa^k = \lambda^k = \delta^k = \frac{l^k}{3} \tag{24}$$

$$\text{if } \frac{6}{Pe} < |u^k| l^k \quad \text{then } \kappa^k = l^k - \frac{4}{|u^k|\,Pe}, \ \lambda^k = \delta^k = \frac{2}{|u^k|\,Pe} \tag{25}$$

with

$$\begin{aligned} \kappa^1 &= \|\mathbf{z}_1^1 - \mathbf{x}_1\|, \quad \lambda^1 = \left\|\frac{\mathbf{x}_1 + \mathbf{x}_2}{2} - \mathbf{z}_2^1\right\|, \quad \delta^1 = \|\mathbf{z}_2^1 - \mathbf{z}_1^1\| \\ \kappa^2 &= \|\mathbf{z}_1^2 - \mathbf{x}_4\|, \quad \lambda^2 = \left\|\frac{\mathbf{x}_3 + \mathbf{x}_4}{2} - \mathbf{z}_2^2\right\|, \quad \delta^2 = \|\mathbf{z}_2^2 - \mathbf{z}_1^2\| \end{aligned} \tag{26}$$

when $u^k \geqslant 0$, while the roles of these points are exchanged when $u^k < 0$. Equations (24) and (25) are based on the work of Brezzi *et al.* [14].

Since Equation (12) is obtained by multiplying the one-dimensional exact-solution-based interpolations in the ξ and η directions, the same strategy can also be applied to the FCBI procedure with link-cutting bubbles. By using the one-dimensional interpolation functions including link-cutting bubbles, which are evaluated on the element lengths h_ξ and h_η defined in Equation (13), the following trial functions in Φ_h can be established in analogy to Equations (12) and (13):

$$\begin{bmatrix} h_1^\phi & h_4^\phi \\ h_2^\phi & h_3^\phi \end{bmatrix} = \mathbf{h}(\alpha')\,\mathbf{h}^{\mathrm{T}}(\beta') \tag{27}$$

$$\text{if } \bar{v}_\xi \geqslant 0 \quad \text{then } \alpha' = \frac{\xi\left\{-\dfrac{\left|Pe_\xi^e\right|}{2}(1-\xi) + 1 + \left|Pe_\xi^e\right|(1-\xi)U_{2\xi}\right\}}{1 + \left|Pe_\xi^e\right|\xi(1-\xi)\left(U_{1\xi} + U_{2\xi}\right)} \tag{28}$$

$$\text{if } \bar{v}_\xi<0 \quad \text{then } \alpha' = \frac{\xi\left\{\dfrac{\left|Pe^e_\xi\right|}{2}(1-\xi)+1+\left|Pe^e_\xi\right|(1-\xi)U_{1\xi}\right\}}{1+\left|Pe^e_\xi\right|\xi(1-\xi)\left(U_{1\xi}+U_{2\xi}\right)} \tag{29}$$

$$\text{if } \bar{v}_\eta \geqslant 0 \quad \text{then } \beta' = \frac{\eta\left\{-\dfrac{\left|Pe^e_\eta\right|}{2}(1-\eta)+1+\left|Pe^e_\eta\right|(1-\eta)U_{2\eta}\right\}}{1+\left|Pe^e_\eta\right|\eta(1-\eta)\left(U_{1\eta}+U_{2\eta}\right)} \tag{30}$$

$$\text{if } \bar{v}_\eta<0 \quad \text{then } \beta' = \frac{\eta\left\{\dfrac{\left|Pe^e_\eta\right|}{2}(1-\eta)+1+\left|Pe^e_\eta\right|(1-\eta)U_{1\eta}\right\}}{1+\left|Pe^e_\eta\right|\eta(1-\eta)\left(U_{1\eta}+U_{2\eta}\right)} \tag{31}$$

with

$$\begin{aligned}
U_{ir} &= \left.\frac{d_1\left(d_1S_{2,2}-d_2S_{1,2}\right)-d_2\left(d_1S_{2,1}-d_2S_{1,1}\right)}{S_{1,1}S_{2,2}-S_{1,2}S_{2,1}}\right|_{ir}|\bar{v}_r| \\
(d_1)_{ir} &= \frac{1}{l_{ir}}\left(\frac{\kappa_{ir}}{2}+\frac{\delta_{ir}}{2}\right), \quad (d_2)_{ir} = \frac{1}{l_{ir}}\left(\frac{\delta_{ir}}{2}+\frac{\lambda_{ir}}{2}\right) \\
\left(S_{1,1}\right)_{ir} &= \frac{1}{Pe}\left(\frac{1}{\kappa_{ir}}+\frac{1}{\delta_{ir}}\right), \quad \left(S_{1,2}\right)_{ir} = -\frac{1}{Pe\delta_{ir}}+\frac{|\bar{v}_r|}{2} \\
\left(S_{2,1}\right)_{ir} &= -\frac{1}{Pe\delta_{ir}}-\frac{|\bar{v}_r|}{2}, \quad \left(S_{2,2}\right)_{ir} = \frac{1}{Pe}\left(\frac{1}{\delta_{ir}}+\frac{1}{\lambda_{ir}}\right) \\
l_{1\xi} &= h_\xi\xi, \quad l_{2\xi} = h_\xi(1-\xi) \\
l_{1\eta} &= h_\eta\eta, \quad l_{2\eta} = h_\eta(1-\eta)
\end{aligned} \tag{32}$$

where $i=1,2$ and $r=\xi,\ \eta$. The two-bubble subgrid in each direction is determined as follows:

$$\text{if } \frac{6}{Pe} \geqslant |\bar{v}_r|\,l_{ir} \quad \text{then } \kappa_{ir}=\lambda_{ir}=\delta_{ir}=\frac{l_{ir}}{3} \tag{33}$$

$$\text{if } \frac{6}{Pe} < |\bar{v}_r|\,l_{ir} \quad \text{then } \kappa_{ir}=l_{ir}-\frac{4}{|\bar{v}_r|\,Pe}, \quad \lambda_{ir}=\delta_{ir}=\frac{2}{|\bar{v}_r|\,Pe} \tag{34}$$

Figure 5 gives an illustration of the trial functions in Φ_h, as per Equation (27). In this figure, for simplicity, a rectangular element is considered. We use the scheme defined by Equation (27) in the numerical example solutions.

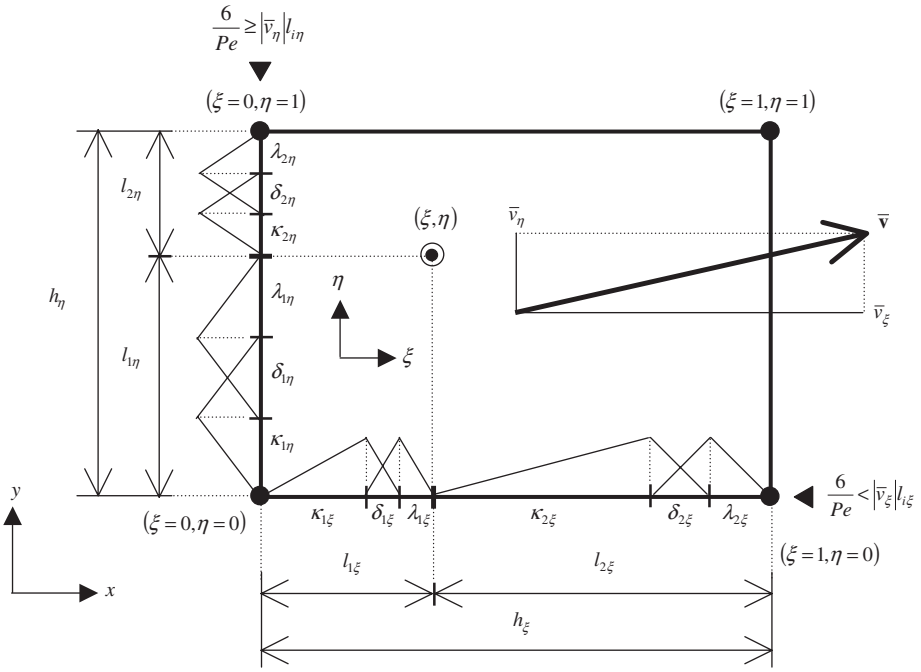

Figure 5. Illustration of the trial functions based on link-cutting bubbles in Φ_h, as per Equation (27).

3. SIMILARITIES BETWEEN THE FORMULATIONS

The direct use of the link-cutting bubbles in the FCBI procedure (see Section 2.3) is based upon the similarities between the original FCBI method and the bubble stabilization. We demonstrate these similarities in the one-dimensional analysis below.

Consider a one-dimensional advection–diffusion problem for which the velocity u and the element length Δx are positive constants. If we use the original FCBI method described in Section 2.1, the following equation is obtained:

$$\left(-\frac{e^{Pe^e}-e^{Pe^e/2}}{e^{Pe^e}-1}-\frac{1}{Pe^e}\right)\theta_{j-1}+\left(\frac{e^{Pe^e}-2e^{Pe^e/2}+1}{e^{Pe^e}-1}+\frac{2}{Pe^e}\right)\theta_j+\left(\frac{e^{Pe^e/2}-1}{e^{Pe^e}-1}-\frac{1}{Pe^e}\right)\theta_{j+1}=0 \tag{35}$$

where the element Péclet number is $Pe^e = Pe\, u \Delta x$. In Equation (35), the temperature in the advection term is interpolated considering the flow condition, while the temperature in the diffusion term is interpolated linearly. Equation (35) can be rewritten in the same form as Equation (17):

$$\left(-\frac{Pe^e}{2}-1-Pe^e U\right)\theta_{j-1}+2\left(1+Pe^e U\right)\theta_j+\left(\frac{Pe^e}{2}-1-Pe^e U\right)\theta_{j+1}=0 \tag{36}$$

with

$$U = \frac{1 - \mathrm{e}^{-Pe^e/2}}{2\left(1 + \mathrm{e}^{-Pe^e/2}\right)} \tag{37}$$

Therefore, Equation (36) can also be the basis of using link-cutting bubbles by substituting for U in Equation (36):

$$U = \frac{d_1\left(d_1 S_{2,2} - d_2 S_{1,2}\right) - d_2\left(d_1 S_{2,1} - d_2 S_{1,1}\right)}{S_{1,1}S_{2,2} - S_{1,2}S_{2,1}}\, u \tag{38}$$

where u^k and l^k used in Equation (23) are, respectively, replaced by u and Δx, and Equation (17) is obtained when $Pe^e = q^k/2$.

In the advection-dominated regime, we see that in the two-bubble subgrid considered in Equation (25) $Pe \to \infty$, $\kappa \to \Delta x$, $\lambda = \delta \to 0$, $uPe\delta = uPe\lambda = 2$. Consequently, we have

$$d_1 \to \tfrac{1}{2}, \quad d_2 \to 0, \tag{39}$$

so that Equation (38) becomes

$$U = \frac{d_1\left(d_1 S_{2,2} - d_2 S_{1,2}\right) - d_2\left(d_1 S_{2,1} - d_2 S_{1,1}\right)}{S_{1,1}S_{2,2} - S_{1,2}S_{2,1}}\, u \to \frac{\frac{1}{4}}{\frac{1}{2}} = \frac{1}{2} \tag{40}$$

As a result, Equation (36) then corresponds to 'full upwinding.' The same can be easily proved using Equation (37); as $Pe^e \to \infty$, $U \to 1/2$. On the other hand, these stabilizing variables approach zero in the diffusion-dominated regime; $Pe^e \to 0$, $U \to 0$ in Equations (37) and (38). As a result, Equation (36) then corresponds to the formulation of the standard Galerkin method in which linear shape functions are used.

Figure 6 shows a comparison of temperature distributions obtained using the exponential scheme, the FCBI method (Equation (35)) and the link-cutting bubbles scheme (Equations (36) and (38)) for the conditions $Pe = 10, 100$ and 10^6. The boundary conditions are

$$\begin{aligned} \theta &= 1 \quad \text{at } x = 0 \\ \theta &= 0 \quad \text{at } x = 1 \end{aligned} \tag{41}$$

The solution is obtained with 30 2-node equal-length elements. As shown, good agreement is obtained in the solution for a wide range of Péclet number problems. The small error in the FCBI temperature solution near $x = 1$ when $Pe = 100$ is due to using the linear temperature interpolation in the diffusion term.

4. NUMERICAL EXAMPLES

In this section we present some solution results that we use to study the stability and accuracy of the FCBI schemes.

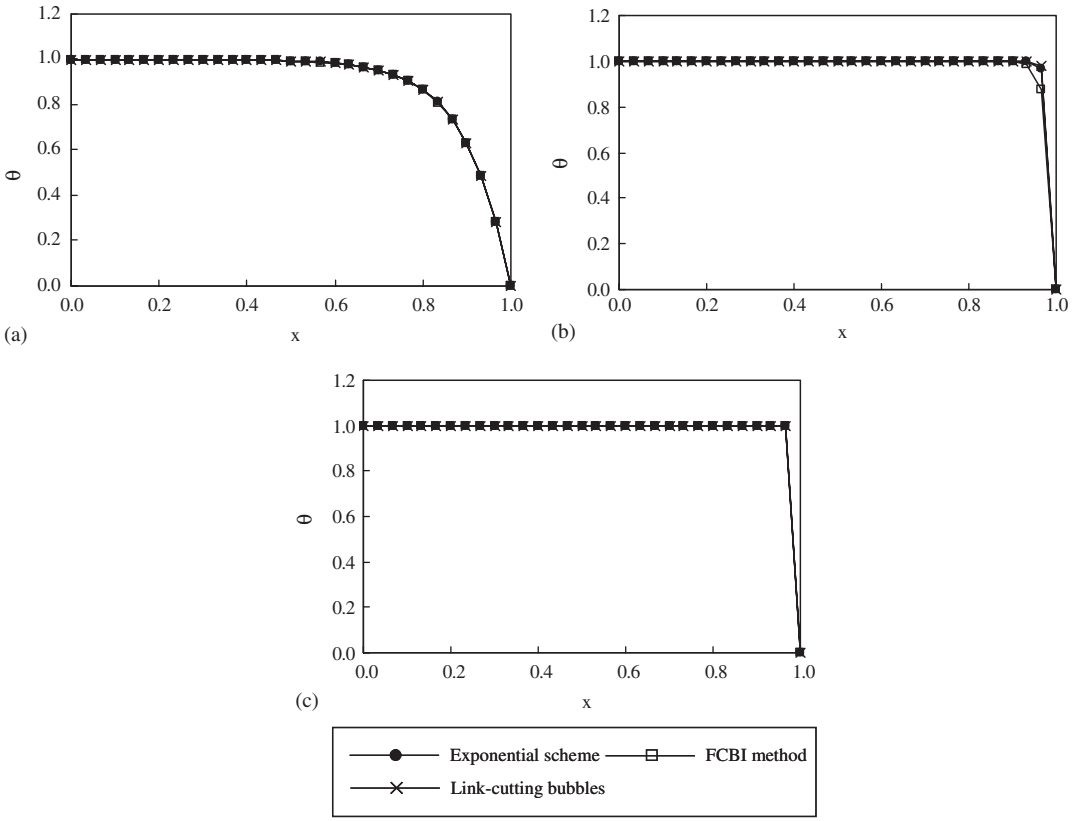

Figure 6. Comparison of temperature values in the one-dimensional advection–diffusion problem: (a) $Pe = 10$; (b) $Pe = 100$; and (c) $Pe = 10^6$.

4.1. Temperature solution in flow between parallel plates

In order to test the proposed FCBI schemes, a temperature-flow problem between parallel plates is analysed. Figure 7 shows the analytical model with the boundary conditions and two meshes of 30×30 elements. The regular mesh and the distorted mesh are used to solve the problem at various Péclet number conditions. When a unit velocity is prescribed in the x direction over the whole domain as shown in Figure 7(a), the exact steady-state solution is

$$\theta(x, y) = \frac{\cos \pi y}{e^a - e^b} \left(e^{a+bx} - e^{b+ax} \right) \tag{42}$$

where

$$a = \tfrac{1}{2} \left(Pe + \sqrt{Pe^2 + 4\pi^2} \right), \quad b = \tfrac{1}{2} \left(Pe - \sqrt{Pe^2 + 4\pi^2} \right) \tag{43}$$

Figures 8 and 9 show the comparison of temperature values on the centre line and temperature profiles on vertical lines, respectively, obtained using the regular mesh. As shown, all of the

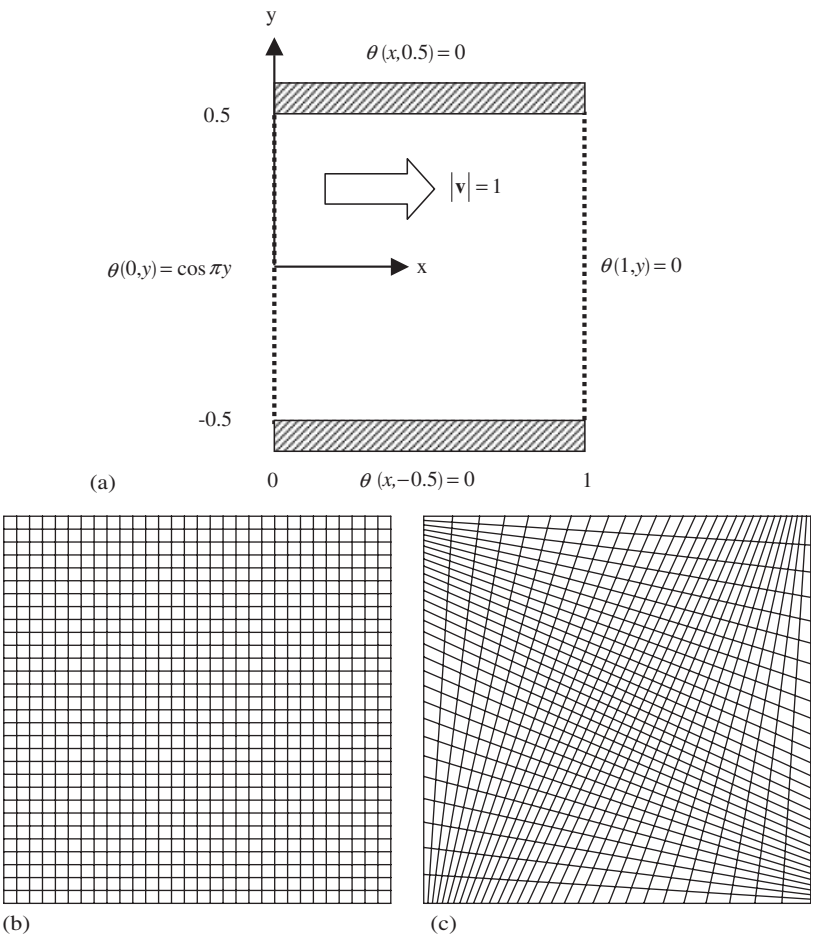

Figure 7. The flow problem between parallel plates and meshes used: (a) problem definition; (b) regular mesh; and (c) distorted mesh.

numerical results calculated with the three FCBI schemes are in good agreement with the exact solutions; the temperature values are only slightly different from the exact solution near the boundary in Figure 8(b) due to the effect of the bilinear interpolation in the diffusion term.

Figures 10 and 11 show the comparison of temperature solutions obtained with the distorted mesh for $Pe = 100$ and 10^6, respectively. The isotherms are distributed at intervals of $(\theta_{\max} - \theta_{\min})/25$. The results calculated with the three FCBI schemes are in good agreement with the exact solution for $Pe = 100$. Good agreement can also be seen in case $Pe = 10^6$ when using the FCBI schemes based on the general solution and the link-cutting bubbles and these schemes give, for the distorted mesh used, clearly more accurate solutions than the original FCBI scheme which predicts a smaller advection effect. The accuracy of the FCBI schemes is also illustrated in Figure 12.

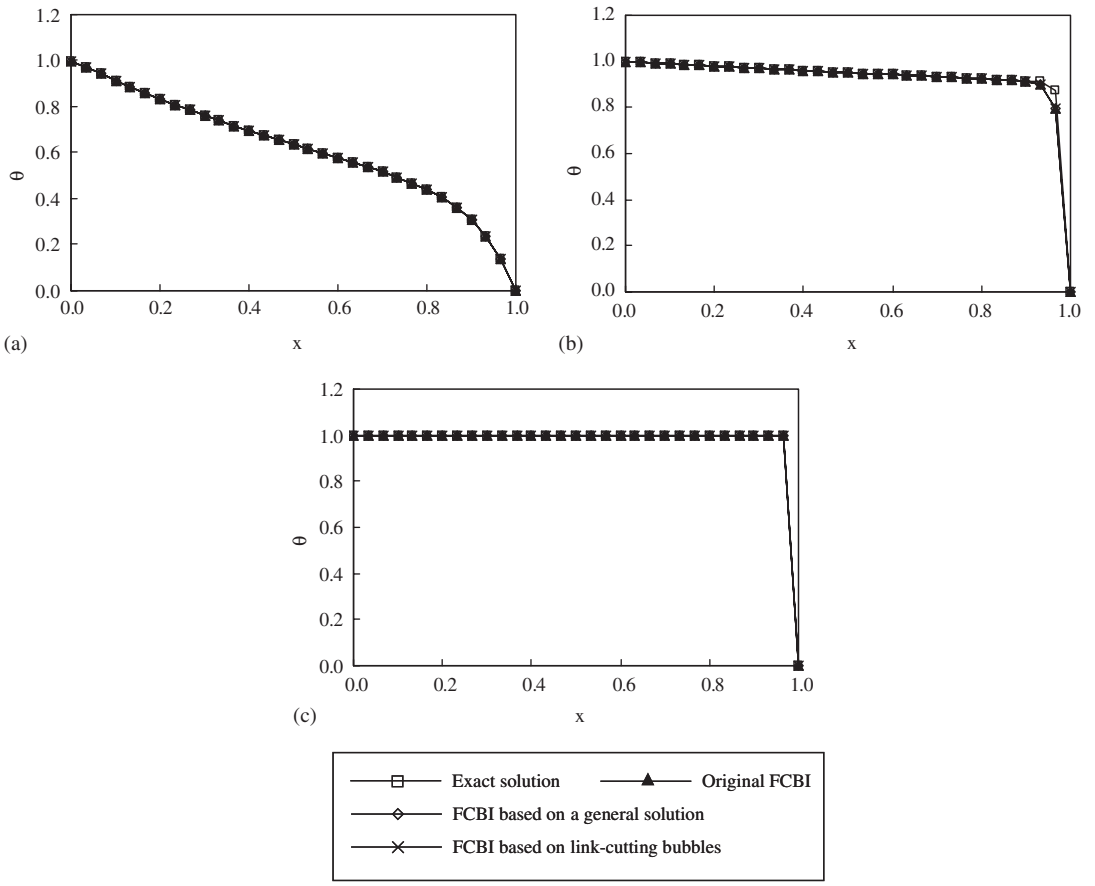

Figure 8. Comparison of temperature values on the centre line obtained with the regular mesh: (a) $Pe = 10$; (b) $Pe = 100$; and (c) $Pe = 10^6$.

4.2. Temperature solutions in flow across a square domain

In the test problem of Section 4.1, the temperature is distributed rather smoothly in the y direction since the temperature boundary condition is given by a cosine function and the velocity component in the y direction is zero. We consider next solutions that are more difficult to obtain when considering high Péclet number conditions due to the discontinuous temperature distributions and a skew advective velocity. The problems are defined in Figure 13. In this analysis, the Dirichlet boundary condition is imposed with the high temperature ($\theta = 1$) and the low temperature ($\theta = 0$). The 45° skew advective velocity, whose magnitude is 1, is prescribed over the whole domain. Therefore, the problem becomes symmetrical with respect to the diagonal line in Case 1, while it is asymmetrical in Case 2. A rather coarse mesh of 12×12 square elements is used for these flow problems, and this mesh is too coarse to reach an accurate solution using the original FCBI scheme when the Péclet number is high. While analytical solutions to the

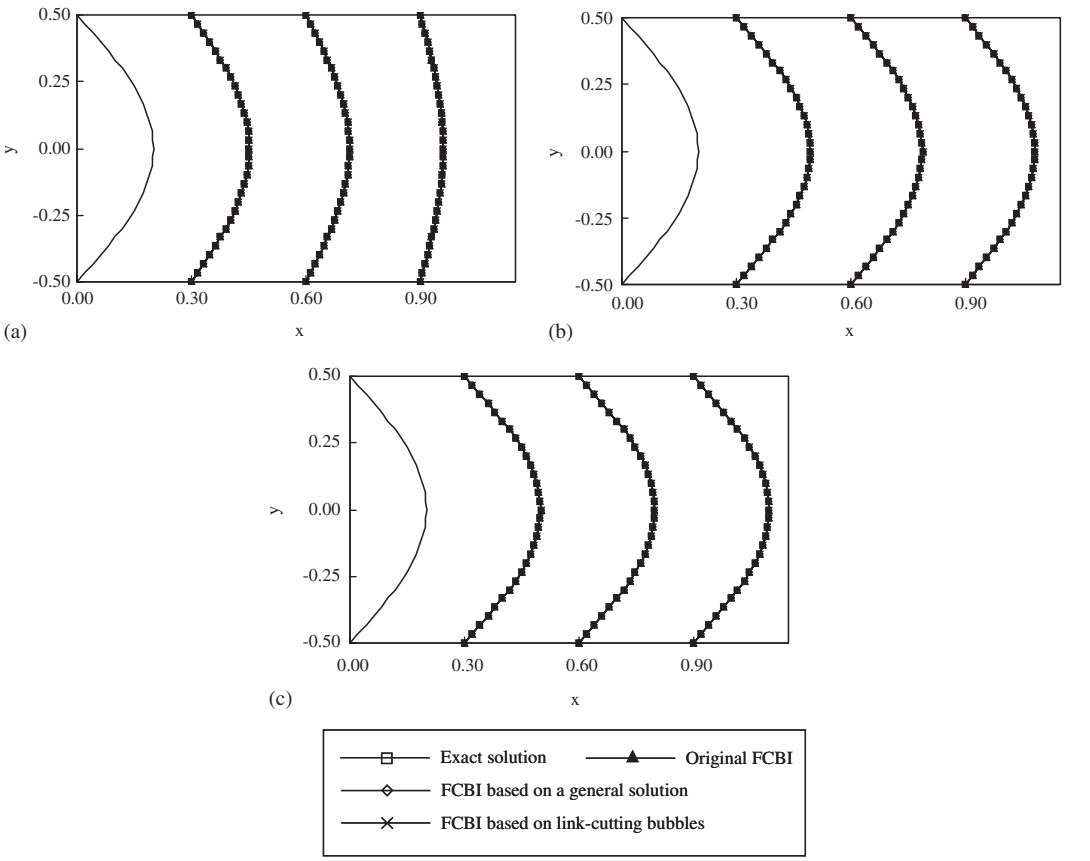

Figure 9. Comparison of temperature profiles on vertical lines obtained with the regular mesh: (a) $Pe = 10$; (b) $Pe = 100$; and (c) $Pe = 10^6$.

problems for intermediate Péclet numbers are not available, of course the solutions for $Pe = 10^6$ are known.

In this case, it is interesting to also obtain the solution using the SUPG scheme. The SUPG formulation is given by the equation

$$\int_\Omega \left(h_i + \frac{k_\gamma}{\|\mathbf{v}\|^2} \mathbf{v}\cdot\nabla h_i \right) \mathbf{v}\cdot\nabla h_j \, \mathrm{d}\Omega\theta_j + \frac{1}{Pe} \int_\Omega \nabla h_i \cdot \nabla h_j \, \mathrm{d}\Omega\theta_j = 0 \tag{44}$$

with h_i the usual isoparametric interpolation functions [16], and

$$k_\gamma = \frac{\gamma}{2Pe} F(\gamma)$$

$$F(\gamma) = \coth\left(\frac{\gamma}{2}\right) - \frac{2}{\gamma}$$

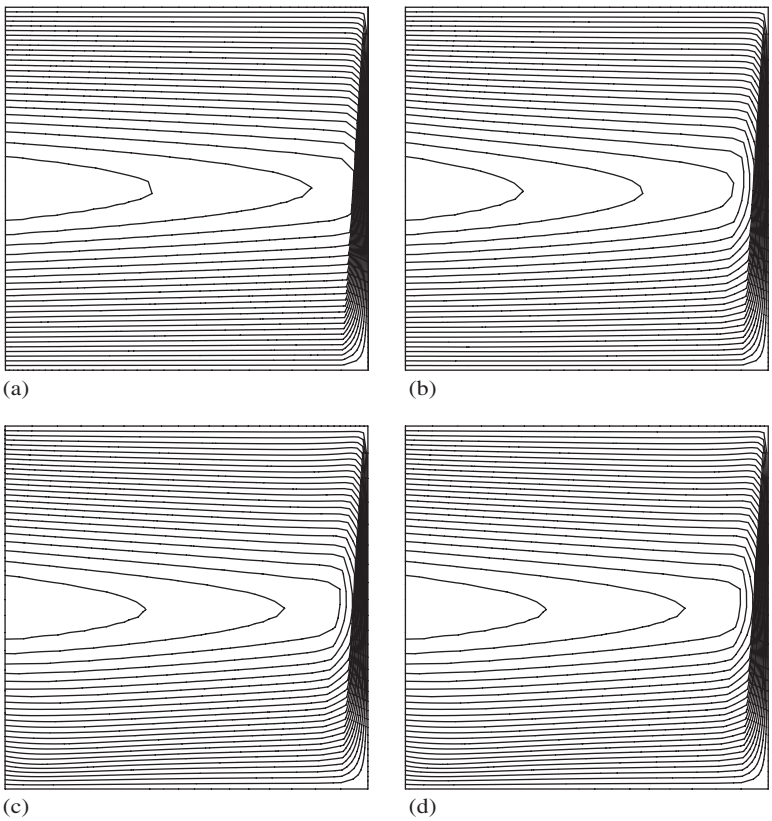

Figure 10. Comparison of temperature solutions obtained with the distorted mesh for $Pe = 100$: (a) exact solution; (b) original FCBI scheme; (c) FCBI scheme based on a general solution; and (d) FCBI scheme based on link-cutting bubbles.

$$\gamma = Pe\sqrt{\left(\bar{v}_\xi h_\xi\right)^2 + \left(\bar{v}_\eta h_\eta\right)^2} \tag{45}$$

where the subscripts i and j denote the global node numbers.

The temperature solutions for $Pe = 100$ calculated with the two proposed FCBI and the SUPG schemes are given in Figure 14. As shown, all the numerical results are similar and the temperature distribution is symmetrical with respect to the diagonal line in Figures 14(a)–(c). The results obtained with the two FCBI schemes are more stable than those obtained with the SUPG scheme since unrealistic behaviour is seen close to the low temperature boundary in Figures 14(c) and (f).

Figure 15 shows the temperature solutions for $Pe = 10^6$. In this case, the temperature changes sharply, indeed discontinuously, on the boundary of the high temperature band due to the very high Péclet number flow. In both cases, the results obtained with the proposed FCBI procedures can be considered accurate in contrast to the results obtained using the SUPG scheme. Of course, further studies of these problems with different meshes and boundary conditions might be pursued and would be valuable.

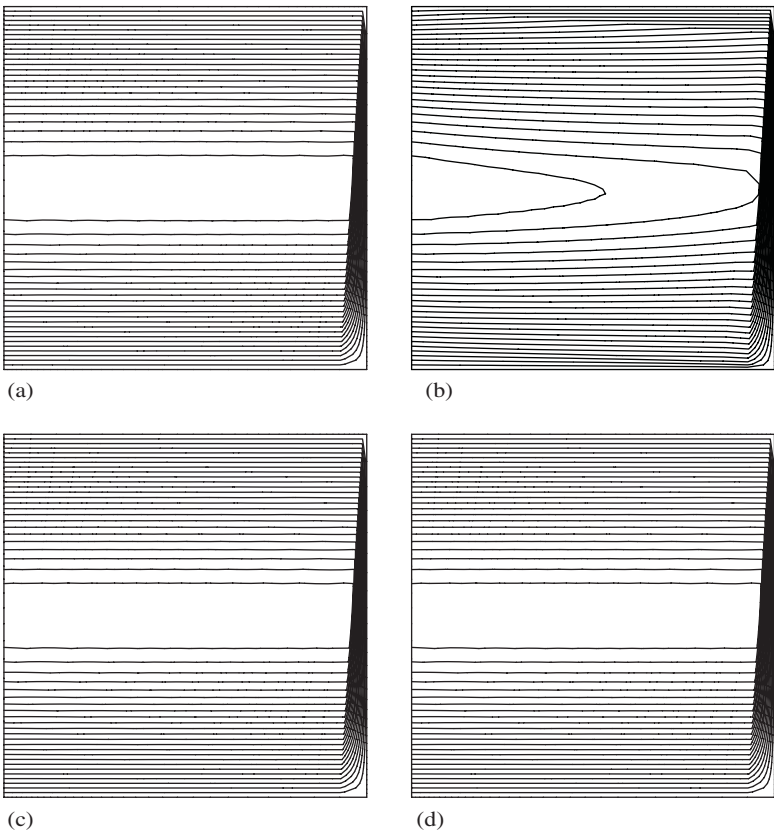

Figure 11. Comparison of temperature solutions obtained with the distorted mesh for $Pe = 10^6$: (a) exact solution; (b) original FCBI scheme; (c) FCBI scheme based on a general solution; and (d) FCBI scheme based on link-cutting bubbles.

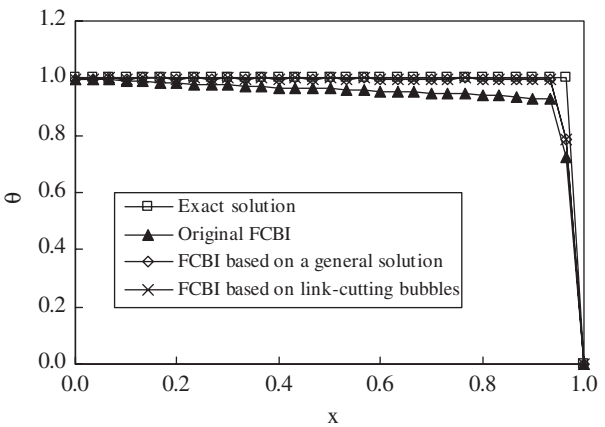

Figure 12. Comparison of temperature values on the centre line obtained with the distorted mesh for $Pe = 10^6$.

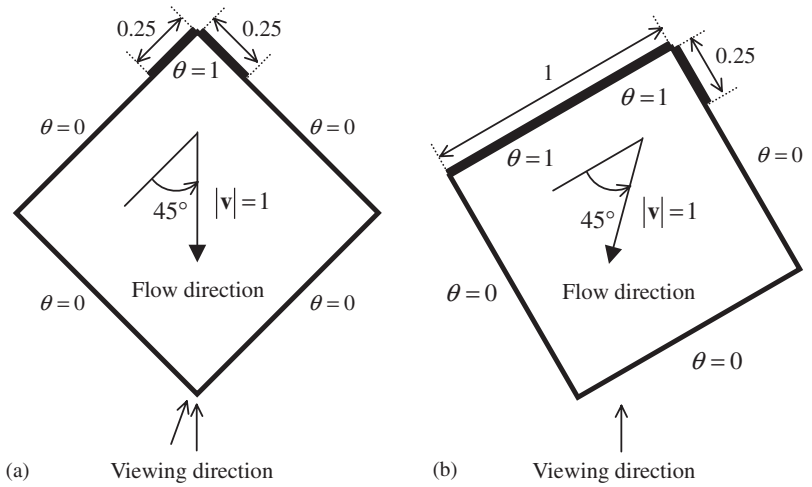

Figure 13. The flow problems with skew advective velocity in a cavity: (a) Case 1; and (b) Case 2.

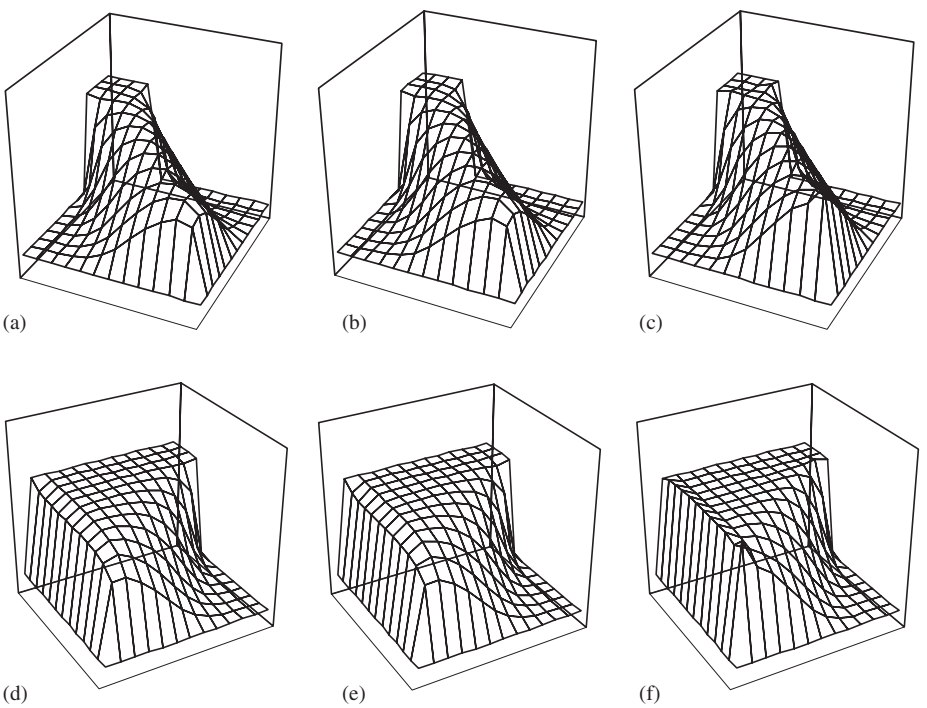

Figure 14. Comparison of temperature solutions for $Pe = 100$: (a) FCBI scheme based on a general solution in Case 1; (b) FCBI scheme based on link-cutting bubbles in Case 1; (c) SUPG scheme in Case 1; (d) FCBI scheme based on a general solution in Case 2; (e) FCBI scheme based on link-cutting bubbles in Case 2; and (f) SUPG scheme in Case 2.

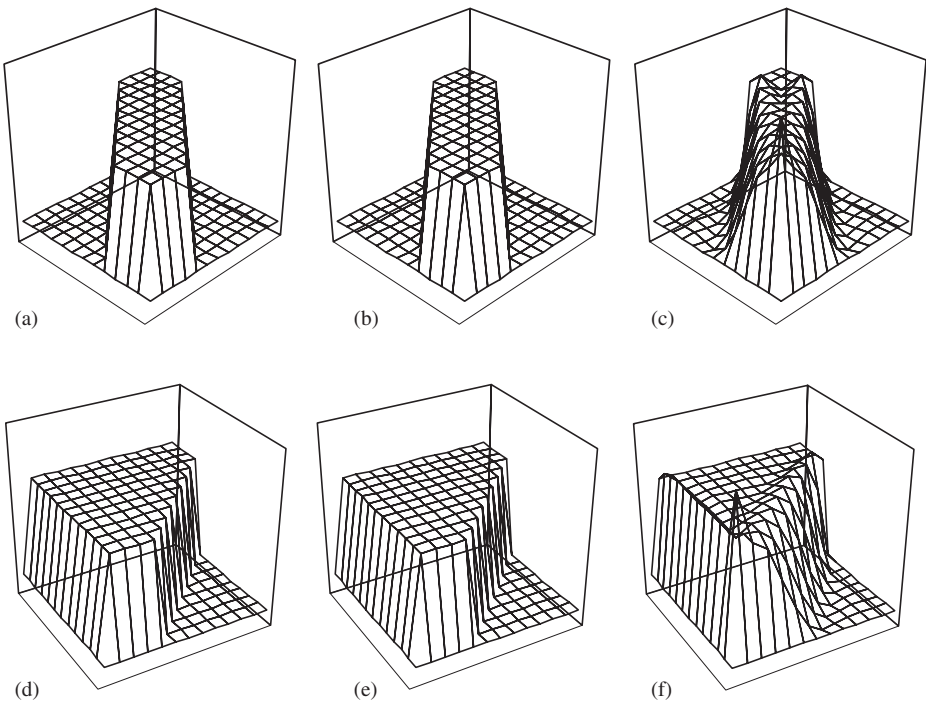

Figure 15. Comparison of temperature solutions for $Pe = 10^6$: (a) FCBI scheme based on a general solution in Case 1; (b) FCBI scheme based on link-cutting bubbles in Case 1; (c) SUPG scheme in Case 1; (d) FCBI scheme based on a general solution in Case 2; (e) FCBI scheme based on link-cutting bubbles in Case 2; and (f) SUPG scheme in Case 2.

5. CONCLUSIONS

We presented in this paper some developments and insight into the FCBI approach for the solution of steady-state advection–diffusion problems. The original FCBI scheme and two additional FCBI procedures were considered. The first additional technique is based on the use of a general solution, and the second additional method is based on the use of the link-cutting bubbles of Brezzi *et al*. The schemes worked quite well in two-dimensional numerical test solutions, in which flows up to the Péclet number 10^6 were considered and also distorted grids were used.

While already used in practice, the FCBI solution approach shows much further potential. Hence additional numerical studies and analytical investigations of FCBI procedures might be pursued, including further developments for complex flow problems. In these developments also ideas used in other techniques should of course be explored.

ACKNOWLEDGEMENTS

We are grateful for the financial support of H. Kohno by the Ministry of Education, Culture, Sports, Science and Technology (MEXT), Japan.

REFERENCES

1. Bathe KJ (ed.). Computational fluid and solid mechanics. *Proceedings of the First MIT Conference on Computational Fluid and Solid Mechanics*. Elsevier: Amsterdam, 2001.
2. Bathe KJ (ed.). Computational fluid and solid mechanics 2003. *Proceedings of the Second MIT Conference on Computational Fluid and Solid Mechanics*. Elsevier: Amsterdam, 2003.
3. Brooks AN, Hughes TJR. Streamline upwind/Petrov–Galerkin formulations for convection dominated flows with particular emphasis on the incompressible Navier–Stokes equations. *Computer Methods in Applied Mechanics and Engineering* 1982; **32**:199–259.
4. Hughes TJR, Franca LP, Hulbert GM. A new finite element formulation for computational fluid dynamics: VIII. The Galerkin/least-squares method for advective–diffusive equations. *Computer Methods in Applied Mechanics and Engineering* 1989; **73**:173–189.
5. Franca LP, Frey SL. Stabilized finite element methods: II. The incompressible Navier–Stokes equations. *Computer Methods in Applied Mechanics and Engineering* 1992; **99**:209–233.
6. Brezzi F, Russo A. Choosing bubbles for advection–diffusion problems. *Mathematical Models and Methods in Applied Sciences* 1994; **4**:571–587.
7. Zienkiewicz OC, Taylor RL. *The Finite Element Method—Volume 3 Fluid Dynamics* (5th edn). Butterworth-Heinemann: Stoneham, MA, 2000.
8. Bathe KJ, Pontaza JP. A flow-condition-based interpolation mixed finite element procedure for higher Reynolds number fluid flows. *Mathematical Models and Methods in Applied Sciences* 2002; **12**:525–539.
9. Bathe KJ, Zhang H. A flow-condition-based interpolation finite element procedure for incompressible fluid flows. *Computers and Structures* 2002; **80**:1267–1277.
10. Bathe KJ, Zhang H. Finite element developments for general fluid flows with structural interactions. *International Journal for Numerical Methods in Engineering* 2004; **60**:213–232.
11. Hendriana D, Bathe KJ. On upwind methods for parabolic finite elements in incompressible flows. *International Journal for Numerical Methods in Engineering* 2000; **47**:317–340.
12. Grätsch T, Bathe KJ. Goal-oriented error estimation in the analysis of fluid flows with structural interactions, in preparation.
13. Yabe T. A universal numerical solver for solid, liquid and gas. In *Proceedings of the First MIT Conference on Computational Fluid and Solid Mechanics*, Bathe KJ (ed.). Elsevier: Amsterdam, 2003; 1424–1425.
14. Brezzi F, Hauke G, Marini LD, Sangalli G. Link-cutting bubbles for the stabilization of convection–diffusion–reaction problems. *Mathematical Models and Methods in Applied Sciences* 2003; **13**:445–461.
15. Bathe KJ. The inf-sup condition and its evaluation for mixed finite element methods. *Computers and Structures* 2001; **79**:243–252,971.
16. Bathe KJ. *Finite Element Procedures*. Prentice-Hall: Englewood Cliffs, NJ, 1996.

